The magnesium transporter NIPAL1 is a pancreatic islet–expressed protein that conditionally impacts insulin secretion

Received for publication, February 28, 2020, and in revised form, May 18, 2020 Published, Papers in Press, May 21, 2020, DOI 10.1074/jbc.RA120.013277

Yousef Manialawy[1], **Saifur R. Khan**[2,3,*], **Alpana Bhattacharjee**[3], **and Michael B. Wheeler**[2,3,*]

From the [1]*Institute of Medical Science and the* [2]*Department of Physiology, University of Toronto, Toronto, Ontario, Canada and the* [3]*Toronto General Hospital Research Institute, University Health Network, Toronto, Ontario, Canada*

Edited by Qi-Qun Tang

Type 2 diabetes is a chronic metabolic disease characterized by pancreatic β-cell dysfunction and peripheral insulin resistance. Among individuals with type 2 diabetes, ~30% exhibit hypomagnesemia. Hypomagnesemia has been linked to insulin resistance through reduced tyrosine kinase activity of the insulin receptor; however, its impact on pancreatic β-cell function is unknown. In this study, through analysis of several single-cell RNA-sequencing data sets in tandem with quantitative PCR validation in both murine and human islets, we identified *NIPAL1* (NIPA-like domain containing 1), encoding a magnesium influx transporter, as an islet-enriched gene. A series of immunofluorescence experiments confirmed *NIPAL1*'s magnesium-dependent expression and that it specifically localizes to the Golgi in Min6-K8 cells, a pancreatic β-cell–like cell line (mouse insulinoma 6 clone K8). Under varying magnesium concentrations, *NIPAL1* knockdown decreased both basal insulin secretion and total insulin content; in contrast, its overexpression increased total insulin content. Although the expression, distribution, and magnesium responsiveness of *NIPAL1* in α-TC6 glucagonoma cells (a pancreatic α-cell line) were similar to the observations in Min6-K8 cells, no effect was observed on glucagon secretion in α-TC6 cells under the conditions studied. Overall, these results suggest that *NIPAL1* expression is regulated by extracellular magnesium and that down-regulation of this transporter decreases glucose-stimulated insulin secretion and intracellular insulin content, particularly under conditions of hypomagnesemia.

Type 2 diabetes (T2D) is a chronic metabolic disease characterized by pancreatic β-cell dysfunction and peripheral insulin resistance (1). Insulin secretion from the β-cell associated with glucose levels is highly dependent on a coordinated pattern of ionic flux events, with the roles of important cations K^+ and Ca^{2+} having been well-established in this process (2–4). However, the relevance of Mg^{2+} to islet secretion and diabetes remains relatively underexplored. This is due in part to the wide variety of roles played by magnesium: it has been implicated in membrane stability, cell growth, energy metabolism, and enzyme activity caused by its role as an ATP-carrying cofactor (4–6). A host of studies have shown that substantial fluxes of Mg^{2+} occur across the plasma membrane under appropriate hormonal or metabolic stimuli (7, 8). However, cellular buffering systems in several models have been found to maintain relatively constant intracellular magnesium levels despite major changes in total magnesium content (9). Exchange is regulated via several Na^+-dependent and independent pathways (9–11); notable transporters include TRPM6/7 (12, 13), MAGT1 (14), the SLC41 (15) and CNNM (16) families, and Golgi-specific MMGT1/2 (17). Of these, TRPM7 and CNNM4 have been found to be the most highly expressed in pancreatic β-cells (18). However, despite transporter activity, ATP complexing remains the most important regulator of free Mg^{2+} (19). It is also worth noting that unlike free Ca^{2+}, cytosolic Mg^{2+} is not likely to act as an intracellular secondary messenger (7).

Overall, the importance of free Mg^{2+} in islets remains unclear. An estimated 30% of patients with T2D are believed to suffer from hypomagnesemia (*i.e.* <0.7 mmol/liter Mg^{2+} in plasma) (20–23). This strong association makes hypomagnesemia a potential risk factor for the development and progression of T2D (18, 24, 25). This may be due in part to the importance of Mg^{2+} in regulating insulin receptor tyrosine kinase activity (22, 26–28), and it has been posited that Mg^{2+} levels are directly linked to insulin resistance and dyslipidemia (20). Two independent meta-analyses have suggested that correcting for hypomagnesemia with long-term oral Mg^{2+} supplementation improves both insulin sensitivity and fasting plasma glucose in T2D patients (29, 30). However, the apparent benefits of added Mg^{2+} may not translate well to islet function.

In vitro studies have demonstrated that pancreatic Mg^{2+} perfusion inhibits both insulin and glucagon secretion, because of magnesium's capacity to disrupt critical Ca^{2+} binding and Ca^{2+} channel activity; this, in turn, alters the sensitivity of these cells to glucose (31–34). The effect of magnesium becomes even more complicated *in vivo*. One study demonstrated that magnesium-deficient rats develop significantly elevated blood-glucose values *versus* pair-fed controls (35); however, another study showed that low dietary Mg^{2+} intake was beneficial in ameliorating high-fat diet–induced obesity in mice, marked by decreased fasting serum glucose levels and improved insulin sensitivity (36). The relevance of Mg^{2+} to islet function thus remains poorly understood.

This article contains supporting information.

* For correspondence: Saifur R. Khan, saifur.khan@utoronto.ca; Michael B. Wheeler, michael.wheeler@utoronto.ca.

In this study, several recent single-cell RNA-sequencing (scRNA-seq) and whole-islet RNA-seq studies were explored to discover novel islet-specific proteins. Through this process, magnesium transporter *NIPAL1* (NIPA-like domain containing 1) was identified in islets and subsequently investigated *in vitro* to determine its relation to pancreatic β-cell function.

Results

Islet-specific candidate selection: NIPAL1

A sequential discovery process was designed to identify novel gene transcripts in pancreatic islets (*i.e.* α- and β-cells) and determine their influence in the secretion of insulin, glucagon, or both (Fig. S1). In the candidate selection phase, 915 candidates were independently investigated and ultimately filtered down into a final shortlist of 28 genes (Fig. 1). The specific publications, data sets, and preprocessing and selection strategies used can be found under "Experimental procedures." The 28 shortlisted genes were investigated in both human and mouse tissues (*i.e.* liver, kidney, islets, and exocrine pancreas) through quantitative real-time PCR (qPCR) to identify those with significant islet enrichment. The transcripts that demonstrated statistically significant higher expression in mouse islets *versus* liver, kidney, and pancreas include *Nipal1*, *Syt13*, *Fam159b*, *Vat1l*, *Syt4*, *Tm4sf4*, and *Tspan13* (Fig. 2*A*). In humans, candidates that demonstrated statistically significant higher expression in islets *versus* liver and pancreas include *NIPAL4*, *IGSF11*, *NIPAL1*, *CYSTM1*, and *BEST3* (Fig. 2*B*). Of all the genes investigated, magnesium transporter *NIPAL1* was the only candidate found to be statistically significant in islets *versus* all other tissues in both species and was thus selected for further characterization and functional investigation using both mouse pancreatic α and β-cell lines (summarized in Fig. 3*A*).

NIPAL1 is concentrated in the Golgi of Min6-K8 cells

Following the identification of *NIPAL1* in both murine and human islets, its expression was similarly assessed via qPCR in Min6-K8 cells (*i.e.* glucose-responsive murine pancreatic β-cell–like cell line). *Nipal1* expression in Min6-K8 cells was comparable with the functionally important gene *Kcnj11*, encoding a K_{ATP} channel that is enriched in β-cells (Fig. 3*B*). In immunofluorescence (IF) studies, abundant NIPAL1 protein expression was also observed in Min6-K8, with a punctate cytosolic distribution suggesting a vesicular presence (Fig. 3*C*). Interestingly, NIPAL1 appeared to be concentrated in an area directly adjacent to the nucleus in all cells. Co-localization studies were thus performed using an antibody against GM-130 (Golgi matrix protein 130) (Fig. 3*D*). A strong overlap between the concentrated region of NIPAL1 and GM-130 indicated that NIPAL1 was indeed most abundant in the Golgi. The co-localization of NIPAL1 was quantified using Pearson's correlation co-efficient (PCC) analysis. Relative co-localization was found to be significantly higher with both insulin granules (0.38 ± 0.04) and the Golgi (0.44 ± 0.04) compared with the nucleus (Fig. 3*E*).

Mg^{2+} enhances NIPAL1 expression in Min6-K8 cells

Because NIPAL1 is a magnesium transporter, experiments were conducted to determine whether NIPAL1 expression in Min6-K8 cells is directly responsive to variations in extracellular magnesium content using qPCR (Fig. 4*A*). The results showed that *Nipal1* gene expression is roughly halved under magnesium-free (0.0 mM) conditions relative to standard (0.8 mM) conditions, with no substantial change under high magnesium (5.0 mM) conditions. These findings thus suggest that *Nipal1* expression depends on the presence of Mg^{2+}. IF studies were performed on cells cultured under similar conditions (Fig. 4*B*). Qualitatively, there was a visible increase in staining intensity under high Mg^{2+} (5.0 mM) within a small area inside each cell (likely the Golgi). Mean NIPAL1 pixel intensity for each condition was thus quantified via ImageJ software analysis (Fig. 4*C*). However, the difference in mean intensity observed between 5.0 and 0.8 mM Mg^{2+} did not reach significance ($p = 0.078$).

NIPAL1 is important for Mg^{2+}-dependent insulin secretion in Min6-K8 cells

To characterize the role of NIPAL1 in pancreatic β-cell function, glucose-stimulated insulin secretion (GSIS) assays were conducted in transfected Min6-K8 cells (*i.e.* NIPAL1 overexpression and knockdown) under both regular and hypo/hypermagnesemic conditions. NIPAL1 overexpression was confirmed via IF using a FLAG antibody (Fig. 5*A*), with mean pixel intensity of both NIPAL1 and FLAG being significantly elevated in cells transfected with NIPAL1 cDNA (Fig. 5*B*) relative to control. In the case of NIPAL1 knockdown using siRNA, qPCR was carried out to evaluate the efficacy of silencing. Results showed a consistent decrease ~70% of expression (or <0.3-fold expression) relative to scramble control (Fig. 5*C*). Attempts were taken to further validate these observations using immune blots; however, the NIPAL1 antibody (used here) was found not suitable for this application (not shown).

In GSIS under standard culture conditions (0.8 mM Mg^{2+}), neither overexpression nor knockdown of NIPAL1 in Min6-K8 cells showed significant alteration in overall insulin secretion (Fig. 6, *A* and *B*). However, it was hypothesized that any observable effect might be magnesium-dependent. In subsequent experiments, the role of NIPAL1 was evaluated under magnesium-induced stress using a range of magnesium concentrations (0.0, 0.4, 0.8, 5.0, and 10.0 mM Mg^{2+}) with 2% FBS (to minimize additional magnesium content) as displayed in Fig. 6*C*, following confirmation that treatments did not impact cell viability (Fig. 6, *I* and *J*); GSIS was performed in both untransfected (Fig. 6*D*) and siRNA-transfected Min6-K8 cells (Fig. 6, *E* and *F*). In untransfected cells, a positive correlation between Mg^{2+} concentration and insulin secretion was readily apparent. (Fig. 6*D*). This suggests an importance for Mg^{2+} in insulin secretion in Min6-K8 cells. In the case of NIPAL1 knockdown, basal insulin secretion (0 mM glucose) was significantly decreased under almost every magnesium concentration (Fig. 6*E*). However, these differences were abolished under treatment with 16.7 mM glucose and KCl (Fig. 6*F*). In addition,

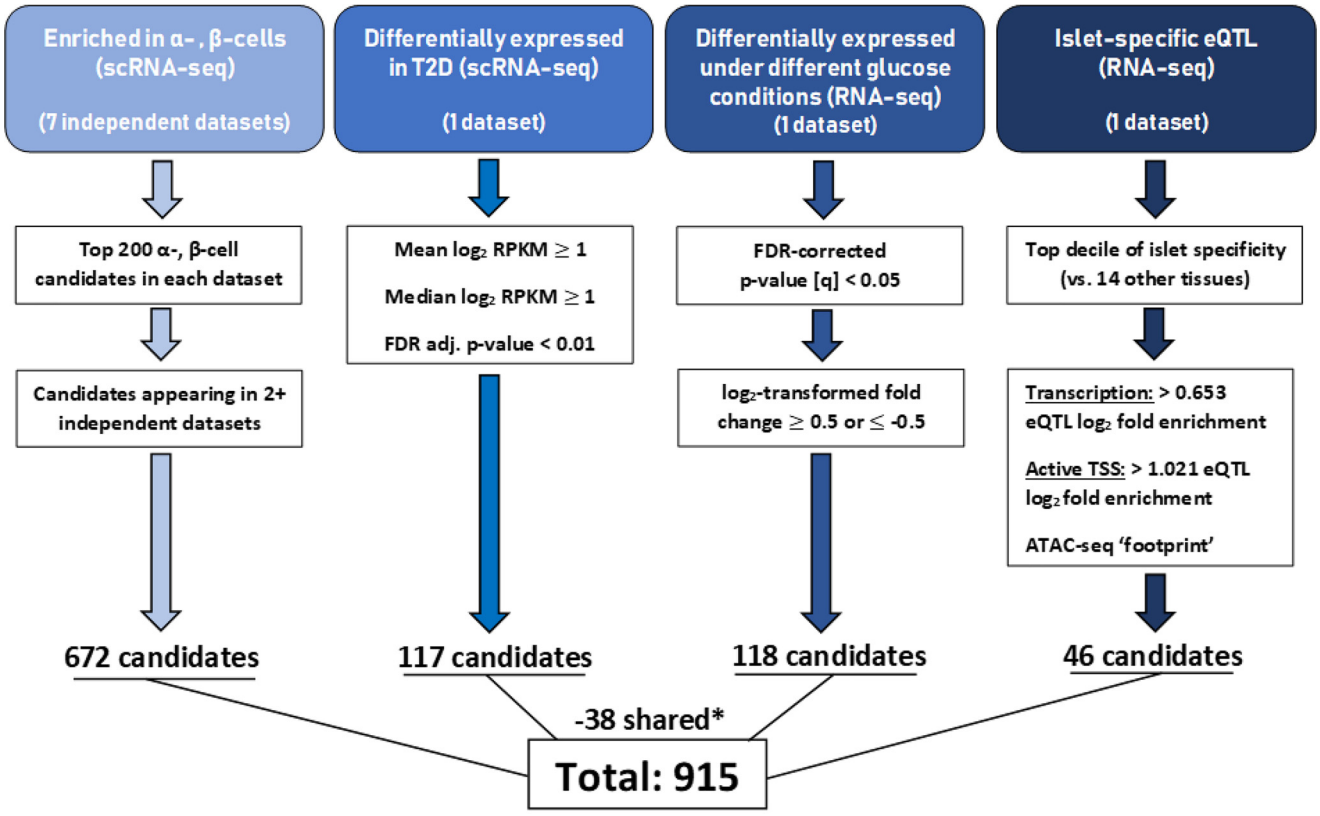

Shortlist criteria:

- ❖ Strong α-/β-cell specificity (> 2x other pancreatic cell types in scRNA-seq) **
- ❖ Islet specificity (3x median of 79 human tissues on BioGPS; ProteinAtlas, GTeXalso used)
- ❖ Novelty in islets (assessed via PubMed search employing broad range of MeSH terms)

Final shortlist: 28

Enriched in α/β	T2D diff. exp.		Glucose diff. exp.		Islet-specific eQTL
C10ORF10	APOH	REEP5	SYT13	BEST3	KCNA6
CNTN1	CPNE3	TMBIM6	SYT4	DOCK1	NIPAL1
CYSTM1	ELAVL4	TSPAN13	TMEM64	ELMO1	NIPAL4
FAM159B	FNBP1L		VAT1L	FITM2	PM20D1
TM4SF4	KCTD12			IGSF11	
	NPTX2			KCNAB2	

* A Venn diagram of shared candidates between sets is in the Supplementary Figures section.

** The 7 independent scRNA-seq datasets were used to assess α/β-cell specificity wherever possible; datasets with weak detection of a candidate (i.e. RPKM < 1) were excluded for this purpose

Figure 1. Overview of candidate selection process to find novel candidates of interest in α- and β-cells. Candidates were taken from seven datasets highlighting the most enriched candidates: one highlighting differentially expressed candidates under T2D, one showing differential expression under glucose induction, and one highlighting islet-specific eQTL. All significance thresholds for log_2-transformed expression and FDR were selected by the studies and were provided in the form of prefiltered lists. A combined total of 915 unique candidates met the initial criteria across all sources. This initial pool was investigated for relative α/β-cell specificity, islet specificity, and novelty in islets. Through this process, the pool of 915 candidates was narrowed down to a final shortlist of 28 candidates, all of which progressed to the next phase of transcriptional validation via qPCR. *MeSH*, medical subject headings; *diff. exp.*, differential expression.

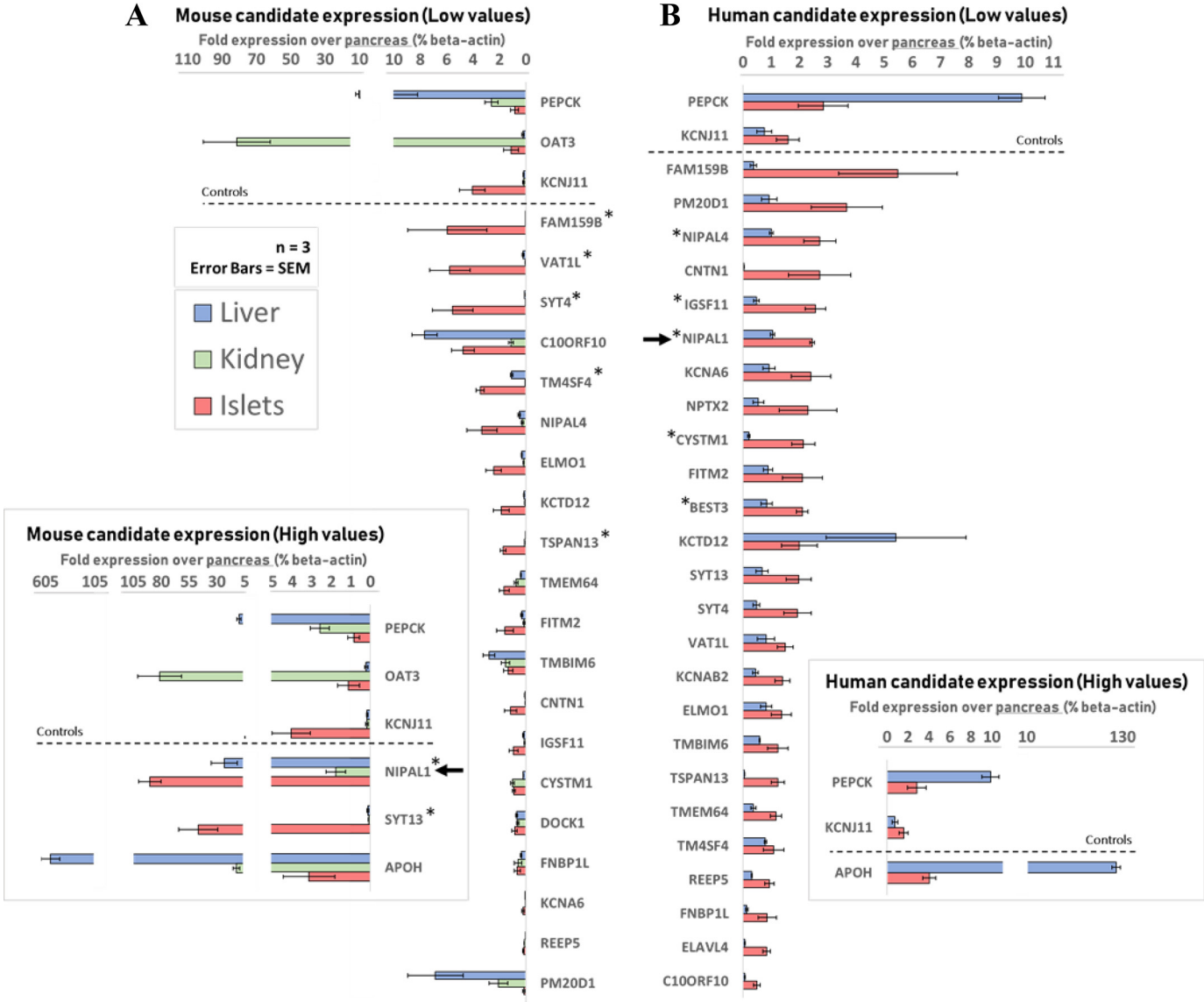

Figure 2. Shortlisted candidate gene expression was measured in mouse (*A*) and human (*B*) tissues via qPCR, with results split into low and high value graphs. In mice, expression was determined in islets, liver, kidney, and exocrine pancreas. In humans, expression was measured in islets, liver, and exocrine pancreas. Raw expression values were normalized to β-actin and then displayed as fold expression over pancreas. The results were then organized by decreasing fold islet expression, after controls *PEPCK* (liver), *OAT3* (kidney), and *KCNJ11* (islet). Candidates that were significantly enriched in islets *versus* all other tissues are indicated (*). *NIPAL1* is significant in both species (indicated by *arrows*). Statistical significance between islets and other tissues was evaluated via one-way analysis of variance and Tukey's honest significant difference (not shown here) (n = 3; values displayed as means ± S.E.).

knockdown of NIPAL1 significantly reduced total insulin content at lower Mg^{2+} concentrations (0.4 and 0.8 mM Mg^{2+}) but not at higher concentrations (5.0 and 10.0 mM Mg^{2+}) (Fig. 6*G*). In contrast, overexpression of NIPAL1 significantly increased total insulin content under almost every concentration (Fig. 6*H*). These observations thus indicate a role for NIPAL1 in insulin secretion and storage in a magnesium-dependent manner.

NIPAL1 is present in the glucagon-producing α-TC cells

The experiments conducted in Min6-K8 cells were additionally carried out in α-TC6 cells (*i.e.* murine α-cell–like cell line, α-TC1 clone 6). *Nipal1* gene expression was observed in α-TC6 as assessed via qPCR, although at notably lower levels than *Kcnj11* (Fig. 7*A*). Follow-up IF experiments confirmed healthy expression at the protein level (Fig. 7*B*). As in Min6-K8, NIPAL1 protein distribution appeared cytosolic and punctate in α-TC cells, with concentration in the Golgi (Fig. 7*C*). PCC analysis of NIPAL1 with glucagon was notable (0.60 ± 0.09), potentially indicating a higher degree of co-localization (Fig. 7*D*). IF experiments of α-TC cells cultured under varying magnesium conditions (Fig. 7*E*) showed stronger NIPAL1 staining under high Mg^{2+} (5.0 mM), which was confirmed to be significantly increased under mean pixel intensity quantification relative to standard Mg^{2+} (0.8 mM) (Fig. 7*F*). In similar fashion to previous GSIS experiments, α-TC6 cells were transfected (*i.e.* NIPAL1 overexpression and knockdown), and both basal glucagon secretion (Fig. 7*G*) and total glucagon were measured (Fig. 7*H*). No

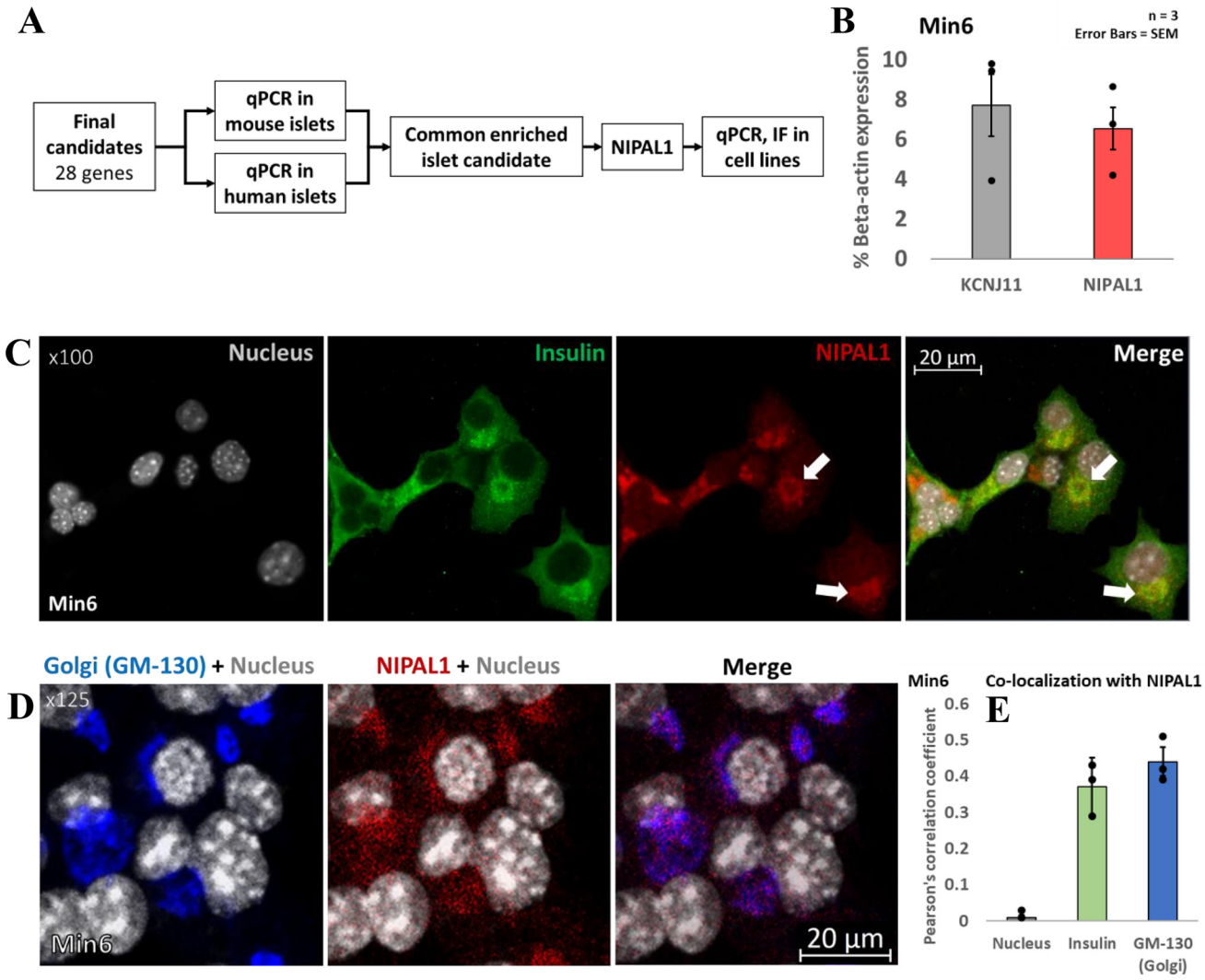

Figure 3. *A*, workflow linking transcriptional validation phase to translational validation phase. *B*, analysis via qPCR identified substantial *Nipal1* expression in Min6-K8 cells, comparable with expression of islet/Min6-enriched potassium channel *Kcnj11* ($n = 3$). *C*, representative images of immunofluorescent staining of NIPAL1 in Min6-K8 cells, co-stained with 4′,6′-diamino-2-phenylindole (DAPI) and insulin. NIPAL1 staining was observed to have a punctate (likely vesicular) presence throughout much of the cytosol but is most concentrated in regions adjacent to the nuclei, as denoted by *arrows*. *D*, subcellular localization studies with GM-130 (Golgi) staining identified that this concentrated region was confined to the Golgi apparatus. However, NIPAL1 still shows distribution outside of the Golgi. *E*, PCC analysis was performed to quantify co-localization between NIPAL1 and other markers ($n = 30$–45 cells across three independent studies; values displayed as means ± S.E.). All IF experiments had $n = 3$.

significant differences were observed between any of the treatment groups with respect to glucagon secretion or content.

NIPAL1's interactome

An interactome was generated based on NIPAL1's known interactions with other proteins. A total of 10 proteins are known to interact with NIPAL1, as follows: MMGT1, MAGT1, PPM1G, SLC35C1, SLC35C2, SLC35B3, TMEM144, FAM35A, NFXL1, and CNGA1 (Fig. 8). Many of these proteins are integrated into membranes (both of the cell and various organelles), with notable representation in the Golgi apparatus and endoplasmic reticulum. (Fig. S3). However, NIPAL1's location is not defined here. In this study, we have shown that NIPAL1 is concentrated in the Golgi. The major suggested biological function of NIPAL1 is transmembrane transport of ions and biomolecules which include Mg^{2+}, carbohydrate derivatives, nucleotide sugars, inorganic cations, metals, and carbohydrates. In addition, NIPAL1 may play a role in glycosylation and in the regulation of the Notch signaling pathway (Fig. S3).

Discussion

A better understanding of T2D pathophysiology entailing the role of various contributing genes/proteins, especially in pancreatic islets, is essential for ultimately devising novel interventions. As such, omics-based technology such as scRNA-seq holds enormous potential to discover novel disease-related factors. In this study, NIPAL1 was identified as a novel islet-enriched protein via a manually curated data mining approach employing several T2D-related scRNA-seq data sets in combination with qPCR validation in both human and murine islets. To understand the functional roles of NIPAL1 in islets, we first examined its expression in α- and β-cell–like cell lines. The abundant expression of *Nipal1* in both α- and β-cell–like cell

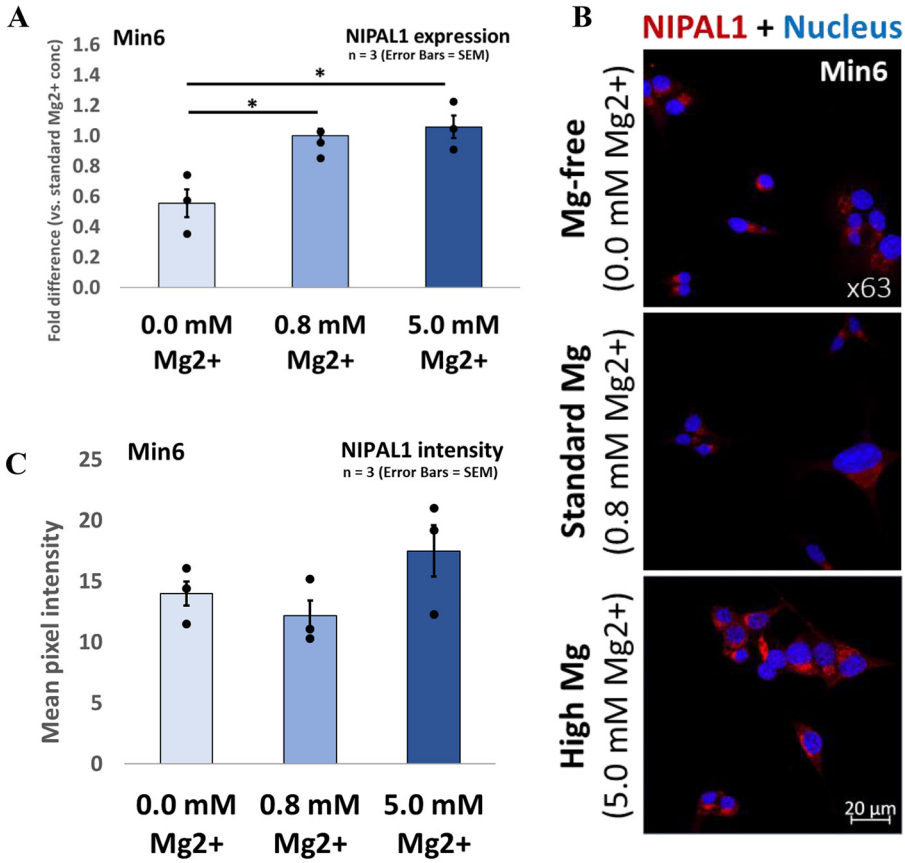

Figure 4. Investigation of effect of magnesium on NIPAL1 expression. *A*, following 24-h culture in standard medium, Min6-K8 cells were cultured in medium with varying Mg^{2+} concentrations (0.0, 0.8, and 5.0 mM), and *Nipal1* gene expression was measured via qPCR. Expression was halved in magnesium-free conditions (0.0 mM) relative to standard conditions (0.8 mM), with no change under high conditions (5.0 mM) ($n = 3$; values displayed as means ± S.E.) *, $p < 0.05$. *B*, IF studies of NIPAL1 expression (×63) were performed under similar conditions. Laser intensities and detection thresholds were kept consistent. NIPAL1 intensity appeared stronger under high Mg^{2+} conditions (5.0 mM), especially adjacent to nuclei (previously identified as Golgi). *C*, average NIPAL1 pixel intensity analysis of defined cell regions was measured to quantify this. Although NIPAL1 intensity appeared to be elevated under 5.0 mM Mg^{2+} relative to 0.8 mM Mg^{2+}, this did not reach significance (p = 0.078) ($n = 30$–45 cells across three independent studies; values displayed as means ± S.E.). *, $p < 0.05$.

lines is supported by observations of robust *Nipal1* expression in murine α- and β-cells in scRNA-seq studies by Benner *et al.* (37) and DiGruccio *et al.* (38). The study of Benner *et al.* in particular places *Nipal1* among its top 200 most enriched murine β-cell candidates. Although the *NIPAL1* rankings in the human study by Segerstolpe *et al.* (39) are unremarkable (12,147th and 13,603rd for β- and α-cells, respectively), it is worth noting that the study by Varshney *et al.* (40) ranks *NIPAL1* within the top decile of human islet specificity when compared with 14 other human tissue types; however, the use of whole-islet RNA-seq prevents the authors from pinpointing specific cell types.

NIPAL1 (NIPA-like domain containing 1) is a magnesium transporter gene, also known as *NIPA3* (nonimprinted in Prader–Willi/Angelman syndrome 3) on account of its structural similarity to paralogs *NIPA1* and *NIPA2*. Although both *NIPA1* and *NIPA2* have been implicated in neurological disorders (41, 42), a role for *NIPAL1*/*NIPA3* as a disease-causing factor remains unestablished. The human Genotype-Tissue Expression database indicates that *NIPAL1* has significant levels of expression in the skin, colon, bladder, and vagina, with more moderate expression in the small intestine and liver; whereas islet data are unavailable on the platform, whole pancreas expression is notably absent (RRID:SCR_013042, accessed June 16, 2019). In mice, the GeneAtlas MOE430 data set on the BioGPS database (ID 152519, accessed April 7, 2020) indicates high Min6 expression and notable expression in thymocytes, stomach, and intestine (islet data are unavailable, but whole pancreas expression is also absent). At present, there are only a handful of publications available that directly reference *NIPAL1*, none of which have studied it in the context of islets or diabetes.

In the present study, NIPAL1 protein was found to have substantial Golgi co-localization and distribution with both insulin and glucagon granules (Figs. 3*E* and 7*D*). It also demonstrated magnesium-dependent expression in Min6-K8 cells (Fig. 4*A*). Insulin secretion experiments revealed that magnesium effectively influenced insulin secretion (Fig. 6*D*). Importantly, knockdown of NIPAL1 expression under hypo- and hypermagnesemic conditions was found to decrease secretion (Fig. 6*E*), and total insulin content was reduced (Fig. 6*G*). In contrast, insulin content was increased with NIPAL1 overexpression (Fig. 6*H*). Although the impact of solely magnesium on total insulin was not measured directly, the recovery of total insulin content under hypermagnesemic (*i.e.* 5.0 and 10.0 mM) conditions to control levels despite NIPAL1 knockdown (Fig. 6*G*) strongly suggests a positive correlation between magnesium and total

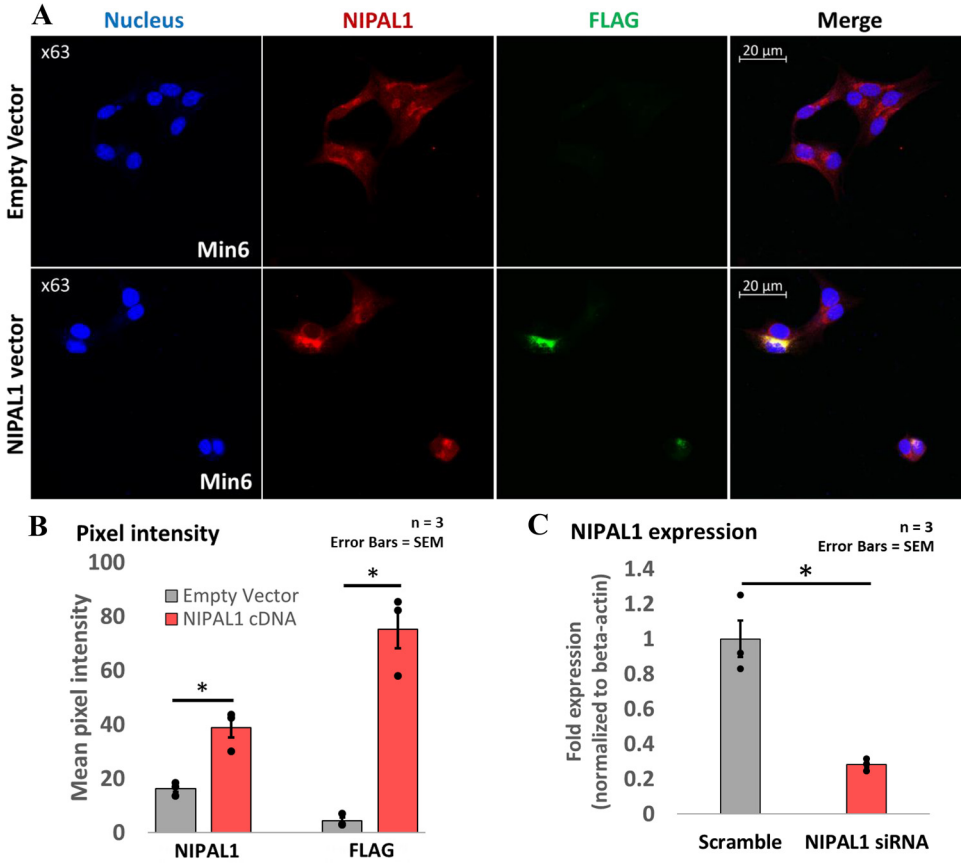

Figure 5. Validation of NIPAL1 overexpression and knockdown. *A*, IF studies of NIPAL1 in Min6-K8 with FLAG epitope antibody were used to confirm overexpression following 24-h transfection of NIPAL1 cDNA-FLAG and empty vectors via Lipofectamine ($n = 3$). *B*, mean pixel intensity quantification confirmed higher intensity for NIPAL1 and FLAG staining under overexpression conditions. *C*, Min6-K8 cells were transfected with either nontargeting scramble siRNA or NIPAL1 siRNA via Lipofectamine, and expression was measured via qPCR; NIPAL1 siRNA fold expression showed ~70% decreased expression compared with scramble ($n = 3$).

insulin in Min6-K8 cells. Although interesting observations were made regarding insulin, no effect was ultimately observed on glucagon secretion in α-TC6 cells (Fig. 7, *G* and *H*). Overall, NIPAL1 appears to be important in promoting cellular insulin content and stabilizing the insulin secretory response in the face of abnormal magnesium levels.

A previous study showed that *Nipal1* expression was upregulated in kidney tissue harvested from mice on a magnesium-restricted diet (43). The results suggested that this increased *Nipal1* expression helps promote Mg^{2+} influx into cells, thereby regulating intracellular magnesium homeostasis when extracellular magnesium is scarce. In contrast, we found that NIPAL1 expression was increased with increasing magnesium levels in Min6-K8 and α-TC6. Furthermore, magnesium-dependent pancreatic β-cell function/sensitivity (Fig. 6*D*) was inhibited under basal conditions with NIPAL1 knockdown (Fig. 6*E*). As such, these islet-specific results indicate that the Mg^{2+} requirement of different tissues varies widely with their functions. Although higher NIPAL1 expression has the potential to allow for higher Mg^{2+} influx, hypermagnesemia, to the best of our knowledge, is not associated with T2D.

The link between Mg^{2+} sensitivity and NIPAL1 expression may potentially be explained by the predicted interaction of NIPAL1 with PPM1G, as displayed in the interactome (Fig. 8). PPM1G is a magnesium-dependent protein phosphatase that has been shown to form protein complexes involved in transcriptional regulation (44). When this is considered alongside its magnesium-dependent function, it is possible then that PPM1G acts as an intermediary sensor between magnesium levels and *NIPAL1* expression.

The detection of NIPAL1 in the Golgi is also of interest. The Golgi is one of the few organelles known to possess its own local magnesium transporters (43), highlighting the importance of Mg^{2+} to Golgi function. Given this, NIPAL1 could play a role in facilitating magnesium entry into the Golgi in a manner that directly impacts the ionic flux governing the trafficking of insulin vesicles within the organelle. A potential driving force may be magnesium's role as a primary ATP-binding co-factor (Mg-ATP) involved in facilitating phosphate transfer reactions (5, 6) that are critical for fueling secretory granule movements (45, 46) and both glycolysis and the citric acid cycle (47, 48). Both Golgi and mitochondrial functions are highly dependent on the availability of ATP delivered by bound magnesium. It is thus possible that higher Mg^{2+} increases Mg-ATP complex formation, which subsequently increases mitochondrial output, insulin granule maturation, and exocytosis. Because NIPAL1 overexpression is specifically observed to increase total insulin content (and knockdown decreases it), greater delivery of magnesium through NIPAL1 may bolster the cell's insulin granule

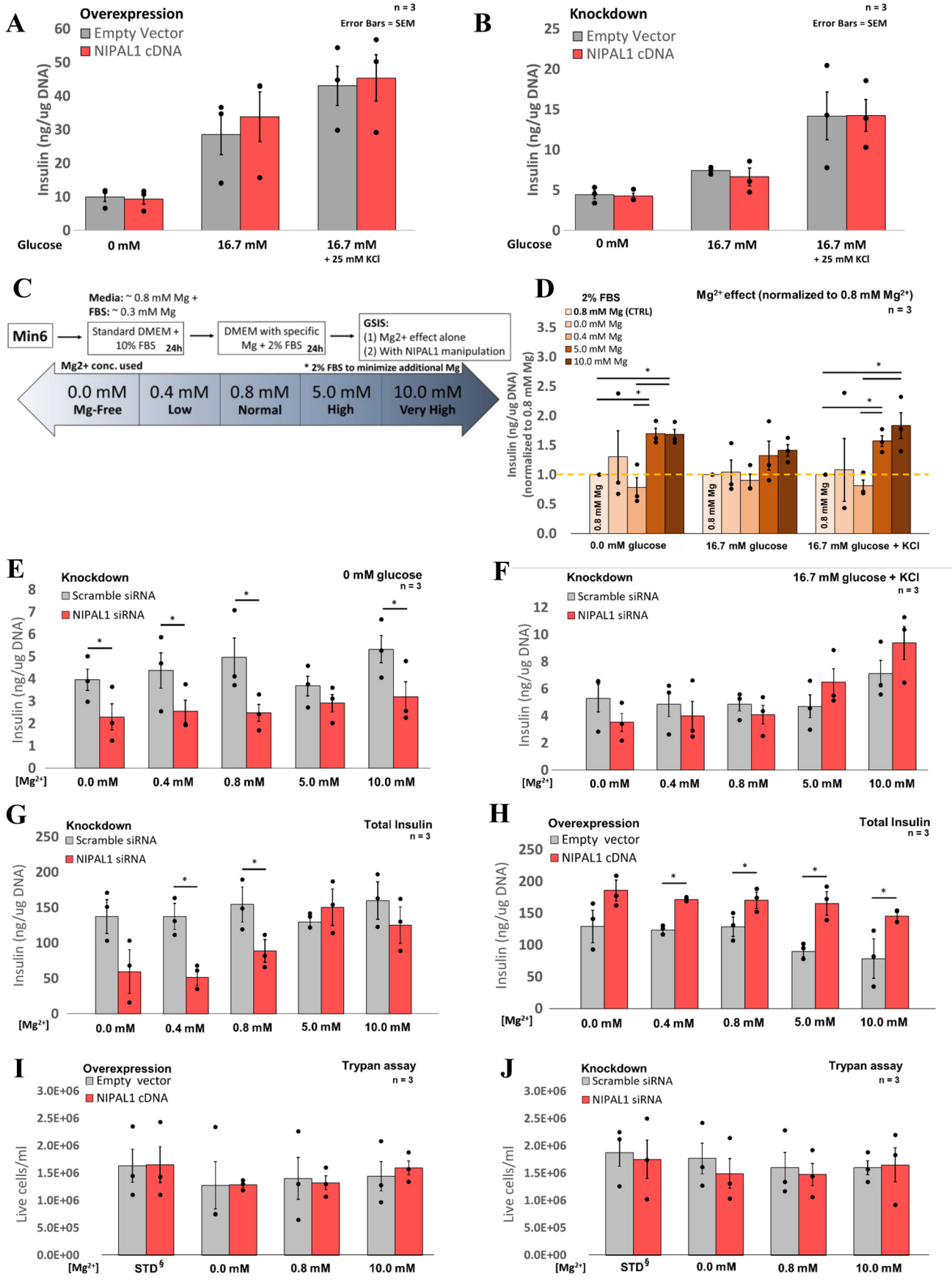
A
Overexpression
Empty Vector
NIPAL1 cDNA
n = 3
Error Bars = SEM
Insulin (ng/ug DNA)
Glucose
0 mM
16.7 mM
16.7 mM + 25 mM KCl
B
Knockdown
Empty Vector
NIPAL1 cDNA
n = 3
Error Bars = SEM
Insulin (ng/ug DNA)
Glucose
0 mM
16.7 mM
16.7 mM + 25 mM KCl
C
Media: ~ 0.8 mM Mg +
FBS: ~ 0.3 mM Mg
Min6
Standard DMEM + 10% FBS 24h
DMEM with specific Mg + 2% FBS 24h
GSIS:
(1) Mg2+ effect alone
(2) With NIPAL1 manipulation
Mg2+ conc. used
* 2% FBS to minimize additional Mg
0.0 mM Mg-Free
0.4 mM Low
0.8 mM Normal
5.0 mM High
10.0 mM Very High
D
2% FBS
Mg2+ effect (normalized to 0.8 mM Mg2+)
n = 3
0.8 mM Mg (CTRL)
0.0 mM Mg
0.4 mM Mg
5.0 mM Mg
10.0 mM Mg
Insulin (ng/ug DNA) (normalized to 0.8 mM Mg)
0.0 mM glucose
16.7 mM glucose
16.7 mM glucose + KCl
E
Knockdown
Scramble siRNA
NIPAL1 siRNA
0 mM glucose
n = 3
Insulin (ng/ug DNA)
[Mg2+]
0.0 mM
0.4 mM
0.8 mM
5.0 mM
10.0 mM
F
Knockdown
Scramble siRNA
NIPAL1 siRNA
16.7 mM glucose + KCl
n = 3
Insulin (ng/ug DNA)
[Mg2+]
0.0 mM
0.4 mM
0.8 mM
5.0 mM
10.0 mM
G
Knockdown
Scramble siRNA
NIPAL1 siRNA
Total Insulin
n = 3
Insulin (ng/ug DNA)
[Mg2+]
0.0 mM
0.4 mM
0.8 mM
5.0 mM
10.0 mM
H
Overexpression
Empty vector
NIPAL1 cDNA
Total Insulin
n = 3
Insulin (ng/ug DNA)
[Mg2+]
0.0 mM
0.4 mM
0.8 mM
5.0 mM
10.0 mM
I
Overexpression
Empty vector
NIPAL1 cDNA
Trypan assay
n = 3
Live cells/ml
[Mg2+]
STD§
0.0 mM
0.8 mM
10.0 mM
J
Knockdown
Scramble siRNA
NIPAL1 siRNA
Trypan assay
n = 3
Live cells/ml
[Mg2+]
STD§
0.0 mM
0.8 mM
10.0 mM

reserve pool, which in turn translates proportionally to greater secretion. Alternatively, increased Mg-ATP formation may influence the ATP:ADP ratio regulating the closure of K_{ATP} channels, whereas extracellular free Mg^{2+} has also been proposed to regulate K_{ATP} channels (49). Fluctuation in extracellular Mg^{2+} levels may also have a substantial effect on membrane potential and by extension the likelihood of triggering secretion.

In summary, this study has demonstrated the importance of magnesium in the preservation of β-cell function as regulated by the magnesium influx transporter NIPAL1, which has been newly identified in islets. Experiments demonstrated that NIPAL1 expression correlates with magnesium and that it is functionally important in permitting magnesium-dependent increases in insulin production and secretion from Min6-K8 cells. However, it is important to emphasize that the importance of NIPAL1 likely only emerges under abnormal conditions such as hypomagnesemia and not under healthy physiological conditions. It is also important in future to further validate the immunofluorescent study results shown here with Western blotting and, particularly in cells where NIPAL1 is ablated, to eliminate any doubt regarding the antibody's specificity. Furthermore, it would be worthwhile to determine whether NIPAL1 influences expression of insulin and other key β-cell genes. In one study, acute lowering of extracellular Mg^{2+} levels in mouse islets and rat INS-1 cells was found not to affect expression of key glucose metabolism genes (*e.g. Gck*, *Abcc8*); knockdown of magnesium transporter *Trpm7* also had no effect on expression of these genes nor that of the *Ins1* gene (50). The same case would thus be expected for NIPAL1. As a final point, further experiments are needed to determine whether magnesium and NIPAL1 are related to glucagon secretion. Overall, these results are pertinent to the emerging role of magnesium in the context of diabetes and dietary metabolism. Further studies investigating NIPAL1 in human pancreatic β-cells may serve to elucidate the role of magnesium in the context of islet health and secretion.

Experimental procedures

Data set selection and basic preprocessing for candidate selection

Several scRNA-seq and traditional RNA-seq studies provided the data sets used for candidate selection in this study (an unpublished scRNA-seq data set from the Wheeler laboratory was additionally included). All data used were acquired in supplementary data sets with results preprocessed or filtered to varying degrees. Specific details can be found in Table 1.

All 915 initially selected candidates were filtered into a final shortlist if they met the following specific criteria: (1) Strong α/β-cell specificity, where mean expression of a candidate was at least double that of other islet (or exocrine) cell types in at least one of the scRNA-seq data sets in which it was identified (where applicable); candidates identified in a whole-islet RNA-seq data set were cross-referenced in scRNA-seq data sets (wherever possible). (2) Strong islet specificity, assessed using the GeneAtlas U133A (gcrma) human tissue data set (79 tissues total) on the BioGPS database. The data set easily distinguishes candidates with mean expression in human islets that is at least triple the median of all tissues, and this was selected as the cut-off point for this criterion. If unavailable on BioGPS, the Genotype-Tissue Expression and ProteinAtlas databases were used to ensure that candidates were not ubiquitously expressed. (3) Novelty in islets was assessed via a thorough PubMed search employing a broad range of medical subject headings terms, *e.g.* "NIPAL1 AND (islet OR diabetes OR pancreas OR pancreatic OR insulin OR glucagon OR secretion)." Candidates with any detailed/focused studies in an islet/diabetes context were deemed not to be novel and excluded. Candidates with no publications were still considered.

Tissue sample acquisition and preparation

Healthy male CD1 mice (8–12 weeks old) were obtained from Charles River and fed a standard chow diet. The mice were housed in the Division of Comparative Medicine facility, University of Toronto. All animal procedures and maintenance were conducted in compliance with protocols approved by the Animal Care Committee at the University of Toronto and the guidelines of the Canadian Council of Animal Care. Liver, kidney, and pancreatic islet and exocrine samples were isolated as described previously (51). If not used immediately, samples were stored at −80 °C. Human samples from six nondiabetic donors (three male and three female; average age, 49.8 ± 16.4 years; average body mass index, 29.8 ± 4.5) were received from either the IsletCore laboratory at the Alberta Diabetes Institute (University of Alberta) or through the Islet Program organized by the Centre for Islet Research, University Health Network. Sample procurement was approved by either the University of Alberta's Human Research Ethics Board or the Research Ethics Boards of the University Health Network (University of Toronto). All human aspects of this study abide by the Declaration of Helsinki principles. Both islets and exocrine tissue were

Figure 6. GSIS experiments in Min6-K8. *A*, 24-h transfection with empty vector or NIPAL1 cDNA was performed via Lipofectamine. Following 1-h incubation in glucose-free KRB medium, GSIS was performed on cells transfected with empty vector or NIPAL1 cDNA using basal (0 mM), high-glucose (16.7 mM), and high-glucose + KCl conditions. Insulin samples were collected after 20-min incubations at 37 °C and measured via HTRF. The results were normalized to DNA. No significant difference was observed between treatment groups under any glucose condition. *B*, 24-h transfection with scramble or NIPAL1 siRNA was performed via Lipofectamine, followed by GSIS as described before, although no significant differences were observed. *C*, Min6-K8 cells were cultured under various Mg^{2+} concentrations. *D*, GSIS was performed. A clear trend was observed between increasing Mg^{2+} concentration and insulin secretion, with significant increases in basal and KCl-induced secretion under 5.0 and 10.0 mM Mg^{2+} treatments. *E*, cells cultured under the same conditions were transfected with non-targeting scramble siRNA or NIPAL1 siRNA. NIPAL1 knockdown was found to significantly decrease basal secretion under all Mg^{2+} concentrations except 5.0 mM. *F*, secretion under NIPAL1 knockdown appeared to be rescued with KCl induction. *G*, NIPAL1 knockdown was also found to decrease total insulin under 0.4 and 0.8 mM Mg^{2+} conditions, but this recovered under hypermagnesemic 5.0 and 10.0 mM Mg^{2+}. *H*, total insulin was also investigated in cells cultured under the same conditions and transfected with either empty vector control or NIPAL1 cDNA. Total insulin was found to be significantly increased under 0.4, 0.8, 5.0, and 10.0 mM Mg^{2+} conditions. *I* and *J*, trypan blue assays confirmed that transfection treatments under varying magnesium conditions with 2% FBS did not impact cell viability or proliferation relative to standard (*STD*) conditions. §, standard conditions = 0.8 mM Mg^{2+} and 10% FBS. All experiments had n = 3 (means ± S.E.). *, $p < 0.05$.

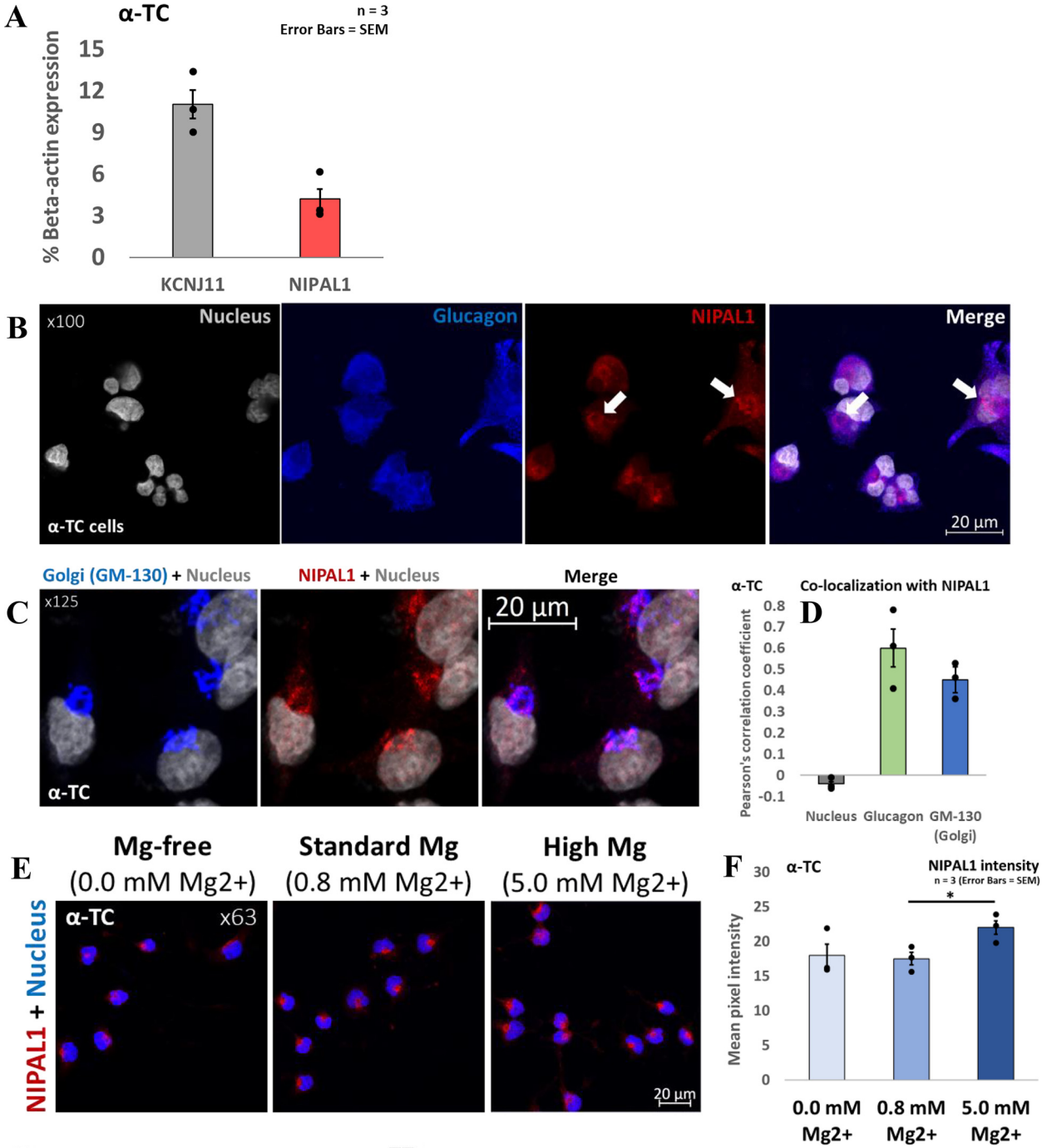
A
α-TC
n = 3
Error Bars = SEM
% Beta-actin expression
15
12
9
6
3
0
KCNJ11
NIPAL1
B
x100
Nucleus
Glucagon
NIPAL1
Merge
α-TC cells
20 µm
C
Golgi (GM-130) + Nucleus
NIPAL1 + Nucleus
Merge
x125
20 µm
α-TC
D
α-TC
Co-localization with NIPAL1
Pearson's correlation coefficient
0.8
0.7
0.6
0.5
0.4
0.3
0.2
0.1
0
-0.1
Nucleus
Glucagon
GM-130 (Golgi)
E
Mg-free (0.0 mM Mg2+)
Standard Mg (0.8 mM Mg2+)
High Mg (5.0 mM Mg2+)
NIPAL1 + Nucleus
α-TC
x63
20 µm
F
α-TC
NIPAL1 intensity
n = 3 (Error Bars = SEM)
*
Mean pixel intensity
30
25
20
15
10
5
0
0.0 mM Mg2+
0.8 mM Mg2+
5.0 mM Mg2+
G
Basal glucagon
n = 3 (Error bars = SEM)
Glucagon (pg/ug DNA)
2.5
2.0
1.5
1.0
0.5
0.0
Empty Vector
NIPAL1 cDNA
Scramble siRNA
NIPAL1 siRNA
H
Total glucagon
n = 3 (Error bars = SEM)
Glucagon (pg/ug DNA)
100
80
60
40
20
0
Empty Vector
NIPAL1 cDNA
Scramble siRNA
NIPAL1 siRNA

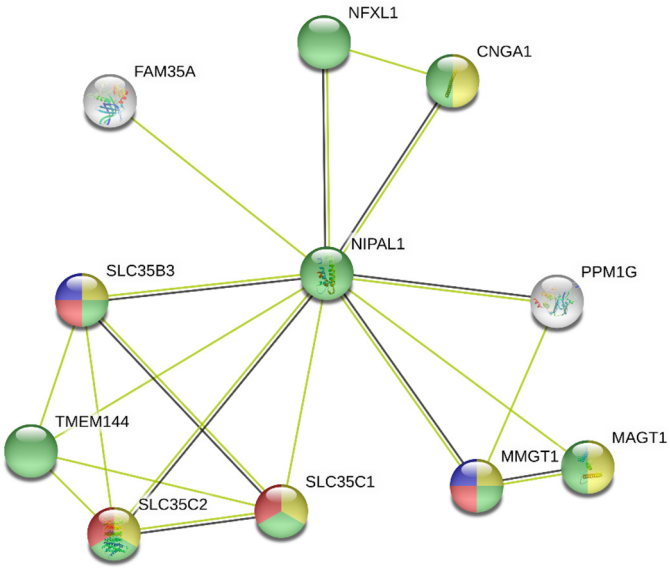

Figure 8. An interactome of the known protein-protein interactions of NIPAL1, constructed with String 11.0 software on a *Homo sapiens* background. Clustering analysis was performed with protein-protein interaction enrichment P value < 0.05 and local clustering co-efficient > 0.85.

handpicked. The samples were cultured or stored in the same manner as mouse samples.

Quantitative PCR—Total RNA was isolated and spectrophotometrically analyzed, reverse transcribed into cDNA, and measured via qPCR analysis as described previously (52). The data were normalized to β-actin mRNA. Primers targeting exon–exon junctions were designed using the NCBI Primer-BLAST tool.

Cell culture and transfection—Min6-K8 cells (a gift from S. Seino [Kobe University, Kobe, Japan] and J. Miyazaki [Osaka University, Suita, Osaka, Japan]) were cultured in high-glucose DMEM (Millipore-Sigma, D6429) supplemented with 10% FBS, 100 units/ml P/S, and 1.75 μl of β-mercaptoethanol. α-TC6 cells were cultured in low-glucose DMEM (Millipore-Sigma, D5921) supplemented with 10% FBS, 100 units/ml P/S, 0.02% BSA, and 15 mM HEPES. The cell lines were maintained at 37 °C and 5% CO_2. For varying magnesium experiments, $MgSO_4$ was dissolved in custom magnesium-free high-glucose DMEM (Wisent) supplemented with 2% FBS (to minimize magnesium content) and 100 units/ml P/S; medium was subsequently filter-sterilized. Following seeding and 24-h culture in standard medium, the cells were washed thrice with magnesium-free PBS and replacement with special magnesium medium was done concurrently with transfection. Transfection was performed for 24 h with Lipofectamine 2000 (Invitrogen, 11668030) according to the manufacturer's instructions. For overexpression, the cells were transfected with empty vector or mouse pCMV6-Nipal1-Myc-DDK (Origene, MR224805). For knockdown, the cells were transfected with either siGENOME nontargeting siRNA pool 1 or siGENOME mouse Nipal1 (Dharmacon, M-054062-01-0005). Cell viability and count was measured using trypan blue and a Countess II automated cell counter (Thermo Fisher, AMQAX1000) according to the manufacturer's instructions.

Immunofluorescence (IF) studies

IF studies in cell lines were performed as described previously (52). The following primary antibodies were used where applicable: mouse anti-glucagon (1:200, Abcam, ab133195), guinea pig anti-insulin (1:100, Dako, A0564), rabbit anti-NIPAL1 (1:200, Abcam, ab17028), mouse anti-FLAG (1:1000, Origene, TA50011), mouse anti-GM-130 (1:1000, BD, 610823, courtesy of Dr. Sergio Grinstein). The secondary antibodies were goat anti-mouse Alexa Fluor®555 (Abcam, ab150114), donkey anti-rabbit Cy5 (Jackson Immunoresearch, 711-175-152), and donkey anti-guinea pig Alexa Fluor®488 (Jackson ImmunoResearch, 706-545-148). The images were acquired on a Zeiss LSM 880 Elyra confocal microscope, and the images were processed in ZEN 2.6 blue edition software. Co-localization analysis of images was performed using the Coloc2 feature of Fiji ImageJ (53) software with 100 Costes randomizations. Relative NIPAL1 intensity was determined by thresholding images to create regions of interest confined to stained cells and then measuring mean pixel intensity of NIPAL1 staining in cells across multiple images (30–50 cells/treatment group).

Glucose-stimulated secretion assay (GSIS) and homogenous time-resolved fluorescence (HTRF)—GSIS was performed on Min6-K8 cells as described previously (54). The insulin samples were stored at −20 °C until HTRF analysis. DNA and total insulin were extracted via acid ethanol. HTRF assays were performed according to the manufacturer's instructions (Cisbio, 62IN2PEG) and read on a PHERAstar plate reader (BMG Labtech). Insulin levels were normalized to DNA.

Glucagon secretion assay and glucagon ELISA

Glucagon samples were collected from α-TC6 cells in similar fashion to GSIS protocols, although without the addition of glucose or KCl; the samples were instead collected without anything added (*i.e.* basal). Collection media included mammalian protease inhibitor to preserve samples. Total glucagon was collected in the same manner as total insulin. Glucagon was measured via an ELISA kit (Sigma, RAB0202) according to the manufacturer's instructions, and the results were normalized to DNA.

Figure 7. A collection of NIPAL1 experiments in α-TC6 cells. *A*, qPCR analysis identified substantial *Nipal1* expression in α-TC6 cells, although at lower levels than islet/α-TC6–enriched potassium channel KCNJ11. *B*, α-TC6 cells were co-stained with NIPAL1, 4′,6′-diamino-2-phenylindole (DAPI), and glucagon/insulin. As in Min6-K8, NIPAL1 was observed to have a punctate (likely vesicular) presence throughout much of the cytosol. *C*, the concentrated regions denoted by *arrows* were confirmed to be localized to the Golgi when co-stained with a GM-130 marker. *D*, PCC analysis was performed to quantify co-localization between NIPAL1 and other markers. PCC = +1 (perfect correlation); PCC = 0 (absence of relationship). *E*, IF studies of cells cultured under varying Mg^{2+} conditions with consistent imaging conditions. *F*, NIPAL1 intensity appeared stronger under high Mg^{2+} conditions (5.0 mM), as confirmed via the significantly higher pixel intensity analysis of NIPAL1 staining in defined cell regions (n = 30–45 cells across three independent studies). *G*, following 1-h incubation in glucose-free KRB medium, the cells were transfected with either empty vector control, NIPAL1 cDNA, scramble siRNA control, or NIPAL1 siRNA, and basal glucagon samples were taken following 20-min incubation. *H*, total glucagon samples were also collected. No significant differences were observed in glucagon secretion or content. All results are displayed as means ± S.E. *, $p < 0.05$ (n = 3).

Table 1
Selected data sets and associated preprocessing for candidate selection

Publication	Application	Islet species	Data set type	Specific data used from Publication	Preprocessing by author	Preprocessing in this study
Benner *et al.* (37)	scRNA-seq	Human and mouse	Most enriched genes	Additional file 12	Mean RPKM values of genes in mouse and human α/β cells	Sorted candidates by decreasing mean RPKM and took top 200 α/β genes for both species
Segerstolpe *et al.* (39)	scRNA-seq	Human	Most enriched genes + differentially expressed under T2D	Tables S1 and S2 (enriched genes) Table S6 (differential expression under T2D)	All tables had mean/median log2RPKM ≥ 1, FDR adjusted $p < 0.01$	Top 200 α/β genes used from enriched tables; α/β tabs of Table S6 used as provided
Xin *et al.* (55)	scRNA-seq	Human and mouse	Most enriched genes	Table S4	Mean RPKM values of genes in mouse and human α/β cells	Sorted candidates by decreasing mean RPKM and took top 200 α/β genes for both species
Li *et al.* (56)	scRNA-seq	Human	Most enriched genes	Data Set SEV6	Mean RPKM values of genes for islet and exocrine cells	Sorted candidates by decreasing mean RPKM and took top 200 α/β genes
DiGruccio *et al.* (38)	scRNA-seq	Mouse	Most enriched genes	File in Gene Expression Omnibus (GSE80673)	Mean log2RPKM values for FACS-sorted cell clusters provided	Cell clusters labeled (matched based on paper details) and sorted in decreasing order of mean expression for α/β (top 200 taken from each group)
Lawlor *et al.* (57)	scRNA-seq	Human	Most enriched genes	Table S6, NonT2D.Beta. *versus* Alpha tab	Mean log2CPM values of genes for α/β cells	Sorted candidates by decreasing mean log2CPM and took top 200 α/β genes
Ottosson-Laakso *et al.* (58)	Whole-islet RNA-seq	Human	Differentially expression under glucose exposure	Tables S4, S5, and S8	FDR-corrected p value [q] $<$ 0.05, mean log2CPM provided	Only included initial candidates with log2-transformed fold change ≥ 0.5 or ≤ -0.5
Varshney *et al.* (40)	Whole-islet RNA-seq	Human (islets + 14 other tissues)	Islet-specific eQTL	Interactive platform: RRID:SCR_018692	Only islet eQTL variants (3314); classified into deciles of islet specificity + epigenetic state	Top decile of islet specificity, default parameters for strong transcription, active TSS, ATAC-seq "footprint"

TSS, Transcription start site; *ATAC-seq*, Assay for Transposase-Accessible Chromatin using sequencing.

Protein–protein interactome

The NIPAL1 interactome was constructed using String 11.0 software (RRID:SCR_005223) on a *Homo sapiens* background. To identify the interacting proteins, a clustering analysis was conducted by keeping protein–protein interaction enrichment p values < 0.05 and average local clustering co-efficient > 0.85. All other analyses such as biological functions (GO), molecular functions (GO), and cellular location (GO) were carried out by setting the false discovery rate (FDR) at <0.05.

Statistical analyses

For qPCR results, one-way analysis of variance and post hoc Tukey's honest significant difference tests were performed to determine statistical significance between islet expression and expression in other tissues. Student's t test was employed for all other statistical analyses. *, $p < 0.05$ was considered statistically significant.

Data availability

All data are available within the manuscript.

Acknowledgments—We acknowledge the Islet Core and the Clinical Islet Laboratory (University of Alberta) for providing human islets from review board-approved donors. Special thanks to Dr. Sergio Grinstein for providing antibodies for co-localization studies.

Author contributions—Y. M., S. R. K., and M. B. W. conceptualization; Y. M. data curation; Y. M. formal analysis; Y. M. validation; Y. M. investigation; Y. M. and S. R. K. visualization; Y. M., S. R. K., and A. B. methodology; Y. M. and S. R. K. writing-original draft; S. R. K. and M. B. W. supervision; S. R. K. and M. B. W. writing-review and editing; M. B. W. funding acquisition.

Funding and additional information—This work was supported by a Canadian Institute for Health Research Grant FRN 143219 (to M. B. W.), a Banting and Best Diabetes Centre Studentship (to Y. M.), and a Diabetes Canada postdoctoral fellowship (to S. R. K.).

Conflict of interest—The authors declare that they have no conflicts of interest with the contents of the article.

Abbreviations—The abbreviations used are: T2D, type 2 diabetes; DMEM, Dulbecco's modified Eagle's medium; eQTL, expressive quantitative trait loci; FBS, fetal bovine serum; FDR, false discovery rate; GSIS, glucose-stimulated insulin secretion; HTRF, homogenous time-resolved fluorescence; IF, immunofluorescence studies; PCC, Pearson's correlation co-efficient; P/S, penicillin/streptomycin; qPCR, quantitative real-time PCR; RPKM, reads per kilobase per million mapped reads; scRNA-seq, single-cell RNA sequencing.

References

1. DeFronzo, R. A., Ferrannini, E., Groop, L., Henry, R. R., Herman, W. H., Holst, J. J., Hu, F. B., Kahn, C. R., Raz, I., Shulman, G. I., Simonson, D. C., Testa, M. A., and Weiss, R. (2015) Type 2 diabetes mellitus. *Nat. Rev. Dis. Primer* **1,** 15019 CrossRef Medline
2. Göpel, S. O., Kanno, T., Barg, S., Eliasson, L., Galvanovskis, J., Renström, E, and Rorsman, P. (1999) Activation of Ca^{2+}-Dependent K^+ Channels

Contributes to Rhythmic Firing of Action Potentials in Mouse Pancreatic β Cells. *J. Gen. Physiol.* **114,** 759–770 CrossRef Medline
3. Liu, Y., Batchuluun, B., Ho, L., Zhu, D., Prentice, K. J., Bhattacharjee, A., Zhang, M., Pourasgari, F., Hardy, A. B., Taylor, K. M., Gaisano, H., Dai, F. F., and Wheeler, M. B. (2015) Characterization of zinc influx transporters (ZIPs) in pancreatic β cells: roles in regulating cytosolic zinc homeostasis and insulin secretion. *J. Biol. Chem.* **290,** 18757–18769 CrossRef Medline
4. de Baaij, J. H. F., Hoenderop, J. G. J., and Bindels, R. J. M. (2015) Magnesium in man: implications for health and disease. *Physiol. Rev.* **95,** 1–46 CrossRef Medline
5. Harrison, W. H., Boyer, P. D., and Falcone, A. B. (1955) The mechanism of enzymic phosphate transfer reactions. *J. Biol. Chem.* **215,** 303–317 Medline
6. Wilson, J. E., and Chin, A. (1991) Chelation of divalent cations by ATP, studied by titration calorimetry. *Anal. Biochem.* **193,** 16–19 CrossRef Medline
7. Romani, A. (2007) Regulation of magnesium homeostasis and transport in mammalian cells. *Arch. Biochem. Biophys.* **458,** 90–102 CrossRef Medline
8. Romani, A. M., and Scarpa, A. (2000) Regulation of cellular magnesium. *Front. Biosci.* **5,** D720–D734 CrossRef Medline
9. Günther, T. (1993) Mechanisms and regulation of Mg^{2+} efflux and Mg^{2+} influx. *Miner. Electrolyte Metab.* **19,** 259–265 Medline
10. Güther, T., Vormann, J., and Förster, R. (1984) Regulation of intracellular magnesium by Mg^{2+} efflux. *Biochem. Biophys. Res. Commun.* **119,** 124–131 CrossRef Medline
11. Cefaratti, C., Romani, A., and Scarpa, A. (1998) Characterization of two Mg^{2+} transporters in sealed plasma membrane vesicles from rat liver. *Am. J. Physiol. Cell Physiol.* **275,** C995–C1008 CrossRef Medline
12. Runnels, L. W., Yue, L., and Clapham, D. E. (2001) TRP-PLIK, a bifunctional protein with kinase and ion channel activities. *Science.* **291,** 1043–1047 CrossRef Medline
13. Schmitz, C., Perraud, A.-L., Johnson, C. O., Inabe, K., Smith, M. K., Penner, R., Kurosaki, T., Fleig, A., and Scharenberg, A. M. (2003) Regulation of vertebrate cellular Mg^{2+} homeostasis by TRPM7. *Cell* **114,** 191–200 CrossRef Medline
14. Goytain, A., and Quamme, G. A. (2005) Identification and characterization of a novel mammalian Mg^{2+} transporter with channel-like properties. *BMC Genomics* **6,** 48 CrossRef Medline
15. Sahni, J., and Scharenberg, A. M. (2013) The SLC41 family of MgtE-like magnesium transporters. *Mol. Aspects Med.* **34,** 620–628 CrossRef Medline
16. Giménez-Mascarell, P., González-Recio, I., Fernández-Rodríguez, C., Oyenarte, I., Müller, D., Martínez-Chantar, M. L., and Martínez-Cruz, L. A. (2019) Current structural knowledge on the CNNM family of magnesium transport mediators. *Int. J. Mol. Sci.* **20,** 11135 CrossRef Medline
17. Goytain, A., and Quamme, G. A. (2008) Identification and characterization of a novel family of membrane magnesium transporters, MMgT1 and MMgT2. *Am. J. Physiol. Cell Physiol.* **294,** C495–C502 CrossRef Medline
18. Gommers, L. M., Hoenderop, J. G., Bindels, R. J., and Baaij, J. H. (2016) Hypomagnesemia in type 2 diabetes: A vicious circle? *Diabetes* **65,** 3–13 CrossRef Medline
19. Cittadini, A., and Scarpa, A. (1983) Intracellular Mg^{2+} homeostasis of Ehrlich ascites tumor cells. *Arch. Biochem. Biophys.* **227,** 202–209 CrossRef Medline
20. Kurstjens, S., de Baaij, J. H., Bouras, H., Bindels, R. J., Tack, C. J., and Hoenderop, J. G. (2017) Determinants of hypomagnesemia in patients with type 2 diabetes mellitus. *Eur. J. Endocrinol.* **176,** 11–19 CrossRef Medline
21. Pham, P.-C. T., Pham, P.-M. T., Pham, S. V., Miller, J. M., and Pham, P.-T. T. (2007) Hypomagnesemia in patients with type 2 diabetes. *Clin. J. Am. Soc. Nephrol.* **2,** 366–373 CrossRef Medline
22. Barbagallo, M., and Dominguez, L. J. (2007) Magnesium metabolism in type 2 diabetes mellitus, metabolic syndrome and insulin resistance. *Arch. Biochem. Biophys.* **458,** 40–47 CrossRef Medline
23. Menzel, R., Pusch, H., Ratzmann, G. W., Besch, W., Förster, F., Albrecht, G., and Ruhnke, R. (1985) Serum magnesium in insulin-dependent diabetics and healthy subjects in relation to insulin secretion and glycemia during glucose-glucagon test. *Exp. Clin. Endocrinol.* **85,** 81–88 CrossRef Medline
24. Dong, J.-Y., Xun, P., He, K., and Qin, L.-Q. (2011) Magnesium intake and risk of type 2 diabetes: meta-analysis of prospective cohort studies. *Diabetes Care* **34,** 2116–2122 CrossRef Medline
25. Kieboom, B. C. T., Ligthart, S., Dehghan, A., Kurstjens, S., de Baaij, J. H. F., Franco, O. H., Hofman, A., Zietse, R., Stricker, B. H., and Hoorn, E. J. (2017) Serum magnesium and the risk of prediabetes: a population-based cohort study. *Diabetologia* **60,** 843–853 CrossRef Medline
26. Nadler, J. L., Buchanan, T., Natarajan, R., Antonipillai, I., Bergman, R., and Rude, R. (1993) Magnesium deficiency produces insulin resistance and increased thromboxane synthesis. *Hypertension* **21,** 1024–1029 CrossRef Medline
27. Suárez, A., Pulido, N., Casla, A., Casanova, B., Arrieta, F. J., and Rovira, A. (1995) Impaired tyrosine-kinase activity of muscle insulin receptors from hypomagnesaemic rats. *Diabetologia* **38,** 1262–1270 CrossRef Medline
28. Vicario, P. P., and Bennun, A. (1990) Separate effects of Mg^{2+}, MgATP, and $ATP4^{-}$ on the kinetic mechanism for insulin receptor tyrosine kinase. *Arch. Biochem. Biophys.* **278,** 99–105 CrossRef Medline
29. Simental-Mendía, L. E., Sahebkar, A., Rodríguez-Morán, M., and Guerrero-Romero, F. (2016) A systematic review and meta-analysis of randomized controlled trials on the effects of magnesium supplementation on insulin sensitivity and glucose control. *Pharmacol. Res.* **111,** 272–282 CrossRef Medline
30. Song, Y., He, K., Levitan, E. B., Manson, J. E., and Liu, S. (2006) Effects of oral magnesium supplementation on glycaemic control in type 2 diabetes: a meta-analysis of randomized double-blind controlled trials. *Diabet. Med.* **23,** 1050–1056 CrossRef Medline
31. Bergsten, P. (1995) Slow and fast oscillations of cytoplasmic Ca^{2+} in pancreatic islets correspond to pulsatile insulin release. *Am. J. Physiol.* **268,** E282–E287 CrossRef Medline
32. Jahnen-Dechent, W., and Ketteler, M. (2012) Magnesium basics. *Clin. Kidney J.* **5,** i3–i14 CrossRef Medline
33. Hermansen, K., and Iversen, J. (1978) Dual action of Mn^{++} upon the secretion of insulin and glucagon from the isolated, perfused canine pancreas: possible interactions with Ca^{++}. *Diabetologia* **15,** 475–479 CrossRef Medline
34. Curry, D. L., Joy, R. M., Holley, D. C., and Bennett, L. L. (1977) Magnesium modulation of glucose-induced insulin secretion by the perfused rat pancreas. *Endocrinology* **101,** 203–208 CrossRef Medline
35. McNeill, D. A., Herbein, J. H., and Ritchey, S. J. (1982) Hepatic gluconeogenic enzymes, plasma insulin and glucagon response to magnesium deficiency and fasting. *J. Nutr.* **112,** 736–743 CrossRef Medline
36. Kurstjens, S., van Diepen, J. A., Overmars-Bos, C., Alkema, W., Bindels, R. J. M., Ashcroft, F. M., Tack, C. J. J., Hoenderop, J. G. J., and de Baaij, J. H. F. (2018) Magnesium deficiency prevents high-fat-diet-induced obesity in mice. *Diabetologia* **61,** 2030–2042 CrossRef Medline
37. Benner, C., van der Meulen, T., Cacéres, E., Tigyi, K., Donaldson, C. J., and Huising, M. O. (2014) The transcriptional landscape of mouse β cells compared to human beta cells reveals notable species differences in long noncoding RNA and protein-coding gene expression. *BMC Genomics* **15,** 620 CrossRef Medline
38. DiGruccio, M. R., Mawla, A. M., Donaldson, C. J., Noguchi, G. M., Vaughan, J., Cowing-Zitron, C., van der Meulen, T., and Huising, M. O. (2016) Comprehensive α, β and δ cell transcriptomes reveal that ghrelin selectively activates δ cells and promotes somatostatin release from pancreatic islets. *Mol. Metab.* **5,** 449–458 CrossRef Medline
39. Segerstolpe, Å., Palasantza, A., Eliasson, P., Andersson, E.-M., Andréasson, A.-C., Sun, X., Picelli, S., Sabirsh, A., Clausen, M., Bjursell, M. K., Smith, D. M., Kasper, M., ämmälä, C., and Sandberg, R. (2016) Single-cell transcriptome profiling of human pancreatic islets in health and type 2 diabetes. *Cell Metab.* **24,** 593–607 CrossRef Medline
40. Varshney, A., Scott, L. J., Welch, R. P., Erdos, M. R., Chines, P. S., Narisu, N., Albanus, R. D., Orchard, P., Wolford, B. N., Kursawe, R., Vadlamudi, S., Cannon, M. E., Didion, J. P., Hensley, J., Kirilusha, A., *et al.* (2017) Genetic regulatory signatures underlying islet gene expression and type 2 diabetes. *Proc. Natl. Acad. Sci. U.S.A.* **114,** 2301–2306 CrossRef Medline

41. Tsang, H. T. H., Edwards, T. L., Wang, X., Connell, J. W., Davies, R. J., Durrington, H. J., O'Kane, C. J., Luzio, J. P., and Reid, E. (2009) The hereditary spastic paraplegia proteins NIPA1, spastin and spartin are inhibitors of mammalian BMP signalling. *Hum. Mol. Genet.* **18,** 3805–3821 CrossRef Medline
42. Xie, H., Zhang, Y., Zhang, P., Wang, J., Wu, Y., Wu, X., Netoff, T., and Jiang, Y. (2014) Functional study of NIPA2 mutations identified from the patients with childhood absence epilepsy. *PLoS One* **9,** e109749 CrossRef Medline
43. Goytain, A., Hines, R. M., and Quamme, G. A. (2008) Functional characterization of NIPA2, a selective Mg^{2+} transporter. *Am. J. Physiol. Cell Physiol.* **295,** C944–C953 CrossRef Medline
44. Gudipaty, S. A., and D'Orso, I. (2016) Functional interplay between PPM1G and the transcription elongation machinery. *RNA Dis.* **3,** e1215 Medline
45. Varadi, A., Ainscow, E. K., Allan, V. J., and Rutter, G. A. (2002) Involvement of conventional kinesin in glucose-stimulated secretory granule movements and exocytosis in clonal pancreatic β-cells. *J. Cell Sci.* **115,** 4177–4189 CrossRef Medline
46. Eliasson, L., Renström, E., Ding, W. G., Proks, P., and Rorsman, P. (1997) Rapid ATP-dependent priming of secretory granules precedes Ca^{2+}-induced exocytosis in mouse pancreatic B-cells. *J. Physiol.* **503,** 399–412 CrossRef Medline
47. Garfinkel, L., and Garfinkel, D. (1985) Magnesium regulation of the glycolytic pathway and the enzymes involved. *Magnesium* **4,** 60–72 Medline
48. Shigematsu, M., Nakagawa, R., Tomonaga, S., Funaba, M., and Matsui, T. (2016) Fluctuations in metabolite content in the liver of magnesium-deficient rats. *Br. J. Nutr.* **116,** 1694–1699 CrossRef Medline
49. Ishizuka, J., Bold, R. J., Townsend, C. M., and Thompson, J. C. (1994) *In vitro* relationship between magnesium and insulin secretion. *Magnes. Res.* **7,** 17–22 Medline
50. Gommers, L. M. M., Hill, T. G., Ashcroft, F. M., and de Baaij, J. H. F. (2019) Low extracellular magnesium does not impair glucose-stimulated insulin secretion. *PLoS One* **14,** e0217925 CrossRef Medline
51. Lee, S. C., Robson-Doucette, C. A., and Wheeler, M. B. (2009) Uncoupling protein 2 regulates reactive oxygen species formation in islets and influences susceptibility to diabetogenic action of streptozotocin. *J. Endocrinol.* **203,** 33–43 CrossRef Medline
52. Wijesekara, N., Dai, F. F., Hardy, A. B., Giglou, P. R., Bhattacharjee, A., Koshkin, V., Chimienti, F., Gaisano, H. Y., Rutter, G. A., and Wheeler, M. B. (2010) β cell-specific Znt8 deletion in mice causes marked defects in insulin processing, crystallisation and secretion. *Diabetologia* **53,** 1656–1668 CrossRef Medline
53. Schindelin, J., Arganda-Carreras, I., Frise, E., Kaynig, V., Longair, M., Pietzsch, T., Preibisch, S., Rueden, C., Saalfeld, S., Schmid, B., Tinevez, J.-Y., White, D. J., Hartenstein, V., Eliceiri, K., Tomancak, P., *et al.* (2012) Fiji: an open-source platform for biological-image analysis. *Nat. Methods* **9,** 676–682 CrossRef Medline
54. Prentice, K. J., Luu, L., Allister, E. M., Liu, Y., Jun, L. S., Sloop, K. W., Hardy, A. B., Wei, L., Jia, W., Fantus, I. G., Sweet, D. H., Sweeney, G., Retnakaran, R., Dai, F. F., and Wheeler, M. B. (2014) The furan fatty acid metabolite CMPF is elevated in diabetes and induces β cell dysfunction. *Cell Metab.* **19,** 653–666 CrossRef Medline
55. Xin, Y., Kim, J., Okamoto, H., Ni, M., Wei, Y., Adler, C., Murphy, A. J., Yancopoulos, G. D., Lin, C., and Gromada, J. (2016) RNA Sequencing of Single Human Islet Cells Reveals Type 2 Diabetes Genes. *Cell Metab.* **24,** 608–615 CrossRef Medline
56. Li, J., Klughammer, J., Farlik, M., Penz, T., Spittler, A., Barbieux, C., Berishvili, E., Bock, C., and Kubicek, S. (2016) Single-cell transcriptomes reveal characteristic features of human pancreatic islet cell types. *EMBO Rep.* **17,** 178–187 CrossRef Medline
57. Lawlor, N., George, J., Bolisetty, M., Kursawe, R., Sun, L., Sivakamasundari, V., Kycia, I., Robson, P., and Stitzel, M. L. (2017) Single-cell transcriptomes identify human islet cell signatures and reveal cell-type-specific expression changes in type 2 diabetes. *Genome Res* **27**:208–222 CrossRef Medline
58. Ottosson-Laakso, E., Krus, U., Storm, P., Prasad, R. B., Oskolkov, N., Ahlqvist, E., Fadista, J., Hansson, O., Groop, L., and Vikman, P. (2017) Glucose-Induced Changes in Gene Expression in Human Pancreatic Islets: Causes or Consequences of Chronic Hyperglycemia. *Diabetes.* **66,** 3013–3028 CrossRef Medline